Check for updates

Geophysical Research Letters

RESEARCH LETTER
10.1029/2024GL111459

On the Size of Dominant Momentum Transporting Eddies in Stable Atmospheric Boundary Layers

Xin Shao[1], **Ning Zhang**[1,2], **Dan Li**[3,4], **and Jianning Sun**[1,5]

[1]School of Atmospheric Sciences, Nanjing University, Nanjing, China, [2]Key Laboratory of Urban Meteorology, China Meteorological Administration, Beijing, China, [3]Department of Earth and Environment, Boston University, Boston, MA, USA, [4]Department of Mechanical Engineering, Boston University, Boston, MA, USA, [5]Joint International Research Laboratory of Atmospheric and Earth System Sciences, Nanjing University, Nanjing, China

Key Points:

- The size of dominant momentum transporting eddies scales with the distance to the ground z in weak stabilities
- The buoyancy influence on energy spectra differs among the three velocities in moderate stabilities
- A new scale different from the Ozmidov scale is proposed to indicate the size of dominant momentum transporting eddies in moderate stabilities

Supporting Information:

Supporting Information may be found in the online version of this article.

Correspondence to:

N. Zhang,
ningzhang@nju.edu.cn

Citation:

Shao, X., Zhang, N., Li, D., & Sun, J. (2024). On the size of dominant momentum transporting eddies in stable atmospheric boundary layers. *Geophysical Research Letters*, *51*, e2024GL111459. https://doi.org/10.1029/2024GL111459

Received 17 JUL 2024
Accepted 15 NOV 2024

© 2024. The Author(s).
This is an open access article under the terms of the Creative Commons Attribution-NonCommercial-NoDerivs License, which permits use and distribution in any medium, provided the original work is properly cited, the use is non-commercial and no modifications or adaptations are made.

Abstract The size of dominant momentum transporting eddies L_{mt} in stable atmospheric boundary layers is poorly understood. This study demonstrates that the distance to the ground z is relevant in constraining L_{mt} in weakly stable conditions ($0 < \zeta < 0.6$, where ζ is the stability parameter) and less relevant in moderately stable conditions ($0.6 < \zeta < 2.0$). The widely used Ozmidov scale, however, fails to represent L_{mt} in moderately stable conditions. The low-wavenumber ends of the $-5/3$ scaling law regions in the spanwise and vertical velocity spectra correlate better with a shear-related length scale. Based on the characteristics of velocity spectra and the balance between kinetic energy and potential energy, a new length scale is proposed to indicate L_{mt} for moderately stable conditions. Observational data show that this new length scale effectively characterizes L_{mt} in moderately stable conditions. These findings can help develop better turbulence parameterization schemes for stable atmospheric boundary layers.

Plain Language Summary The size of dominant momentum transporting eddies L_{mt} in stable atmospheric boundary layers is poorly understood. This study proposes a new length scale to characterize L_{mt} when the influence of the Earth's surface is negligible. These findings have significant implications for developing better turbulence parameterization schemes for stable atmospheric boundary layers.

1. Introduction

While extensive effort has been devoted to developing turbulence closure schemes for stable atmospheric boundary layers (Grachev et al., 2013; Katul et al., 2011, 2014; Li, 2020; Li et al., 2016; Mahrt, 2014; Mellor & Yamada, 1974; Monin & Obukhov, 1954; Zilitinkevich et al., 2007, 2013), operational weather and climate models still have difficulties in reproducing key features of stable boundary layers (Sandu et al., 2013). One of the most uncertain aspects associated with current theories and closure schemes of stably stratified turbulence is the size of dominant momentum transporting eddies L_{mt} (Zilitinkevich et al., 2013). Under neutral conditions, there is a consensus that L_{mt} is proportional to the distance to the ground z due to geometric constraints (Drobinski et al., 2004; Ghannam et al., 2018; Guala et al., 2011; Katul et al., 2013; Klipp, 2014; Krug et al., 2019; Marusic & Monty, 2019; Townsend, 1976). However, how L_{mt} behaves for stably stratified turbulence is less clear, although it is expected that L_{mt} should decrease because the movement of air parcels is constrained by the stratification.

Motivated by Monin-Obukhov similarity theory (MOST) (Monin & Obukhov, 1954), it might be tempting to assume that L_{mt} is the function of the stability parameter ζ (Ayet & Katul, 2020; Ji & Chen, 2023; Katul et al., 2011; Salesky et al., 2013). There have been recent developments in this direction. For instance, Katul et al. (2011) and Salesky et al. (2013) used the vertical integral length scale to approximate L_{mt} and formulated the dependence of L_{mt} on ζ. The variation of L_{mt} with ζ was then incorporated into a theoretical framework to predict the behavior of the non-dimensional wind shear $\phi_m = \kappa z S/u_*$, where $\kappa = 0.4$ is the Karman constant, S is the mean wind shear, and u_* is the friction velocity. Note that in MOST, ϕ_m is only a function of ζ and the widely accepted empirical form of $\phi_m(\zeta)$ is the Businger-Dyer relation $\phi_m(\zeta) = 1 + \beta_m \zeta$ where $\beta_m \approx 5$ (Businger et al., 1971; Dyer, 1974; Foken, 2006; Högström, 1988). Nevertheless, the predicted $\phi_m(\zeta)$ by Katul et al. (2011) and Salesky et al. (2013) deviates from the Businger-Dyer relation under moderately stable conditions, indicating that the vertical integral length scale may not be a good indicator for the size of dominant momentum transporting eddies under such conditions. This is not too surprising given that their theoretical framework relies on the assumed dependence of L_{mt} on z. However, when ζ is sufficiently high, turbulent eddies are expected to be not

19448007, 2024, 23, Downloaded from https://agupubs.onlinelibrary.wiley.com/doi/10.1029/2024GL111459, Wiley Online Library on [20/12/2024]. See the Terms and Conditions (https://onlinelibrary.wiley.com/terms-and-conditions) on Wiley Online Library for rules of use; OA articles are governed by the applicable Creative Commons License

affected by the wall and hence turbulent statistics are independent on z (i.e., the so-called z-less scaling) (Holtslag & Nieuwstadt, 1986; Shi & Hu, 2020; Sun et al., 2012, 2016).

Under moderately stable conditions where z becomes a less constraint on turbulent transport, the buoyancy frequency N becomes a more compelling parameter in constraining L_{mt}. Some studies attempted to characterize L_{mt} using length scales that are directly related to N, such as the vertical buoyancy length scale $L_{wN} = \sigma_w/N$ (Sorbjan, 2006) and the Ozmidov length scale $L_{oz} = \left(\epsilon/N^3\right)^{1/2}$ (Dougherty, 1961; Grachev et al., 2015; Li et al., 2016; Ozmidov, 1965), where σ_w and ϵ denote the standard deviation of vertical velocity and the turbulence dissipation rate, respectively. In particular, L_{oz} is commonly used in oceanography to indicate the largest isotropic eddy (Caulfield, 2021; Mater et al., 2013; Mater & Venayagamoorthy, 2014a, 2014b). In atmospheric boundary layer studies, Li et al. (2016) found that the predicted $\phi_m(\zeta)$ by the same theoretical framework as described in Katul et al. (2011) and Salesky et al. (2013) is in better agreement with observational data when considering the constraint of L_{oz} on L_{mt} under mildly to moderately stable conditions. However, the applicability and limitations of L_{oz} in characterizing L_{mt} have not been thoroughly examined.

This study aims to examine the applicability and limitations of L_{oz} in constraining L_{mt}, thereby providing a comprehensive characterization for L_{mt} in stably stratified turbulence. Strong stabilities ($\zeta > 2$) are excluded in this study because turbulence mixing is suppressed and mesoscale waves play a significant role at these stabilities (Acevedo et al., 2016; Lan et al., 2018; Peltola et al., 2021; Shao et al., 2023; Sun et al., 2012, 2016, 2020; Van de Wiel et al., 2012). In the following, details of data set, data processing, and length scales constructed from the parameter space are elaborated in Section 2; results are presented in Section 3; conclusions and discussion can be found in Section 4.

2. Data and Methods

2.1. Data

Data with a sampling frequency of 20 Hz from the Cooperative Atmosphere-Surface Exchange Study (CASES-99) in October 1999 (Poulos et al., 2002) are used in this study. There were eight three-dimensional sonic anemometers (CSAT version 3, Campbell Scientific, USA) on a 60-m tower at 1.5, 5, 10, 20, 30, 40, 50, and 55 m. The lowest one was moved to 0.5 m from 1.5 m on 20 October. Air temperature was measured by Väisälä temperature sensors (Väisälä 50Y Humitter) with a sampling frequency of 1 Hz at six heights (5, 15, 25, 35, 45, and 55 m). The tower site was surrounded by relatively flat terrain.

2.2. Data Processing

The coordinate system is defined that x, y, and z-coordinates represent the streamwise direction, the spanwise direction, and the vertical direction, respectively, and the corresponding velocity components are u, v, and w. Data are split into 15-min segments for turbulence variables calculation. The mean wind shear is defined as $S = \frac{\partial U}{\partial z}$, where $U = \overline{u}$ is the mean wind speed with the overbar representing the time average. The buoyancy frequency is defined as $N = \left(\frac{g}{\theta}\frac{\partial \overline{\theta}}{\partial z}\right)^{\frac{1}{2}}$, where θ denotes the potential temperature and g is the gravity acceleration. Both wind speed gradient and potential temperature gradient are computed by fitting polynomial functions to the mean wind speed and the mean potential temperature profiles. The turbulence dissipation rate ϵ is obtained by fitting the relation $S_2(r) = 2.13\epsilon^{2/3}r^{2/3}$ (Kolmogorov, 1941), where $S_2(r) = \overline{\left(u\left(t + \frac{r}{U}\right) - u(t)\right)^2}$ with t denoting the time and r denoting the separation scale following Taylor's frozen eddy hypothesis. The friction velocity is computed as $u_* = \sqrt{-\overline{u'w'}}$ and the stability parameter is computed as $\zeta = -\frac{\kappa z g \overline{w'\theta'}}{\theta u_*^3}$. The spectrum and co-spectrum are computed by employing continuous wavelet transform first and then adding up the wavelet coefficients over time at specific scales. The Daubechies Wavelet D4 (db4) is used to compute continuous wavelet transform and the Welch's method (Welch, 1967) is employed to smooth the results.

2.3. The Size of Dominant Momentum Transporting Eddies

In this study, we characterize the size of dominant momentum transporting eddies L_{mt} using the wavenumber (k_{mt}) at which the peak of pre-multiplied co-spectrum of turbulent momentum flux occurs: $L_{mt} = 1/k_{mt}$. We choose to use k_{mt} because k_{mt} characterizes the most energetic scale in momentum transport (Pope, 2000). As examples, the

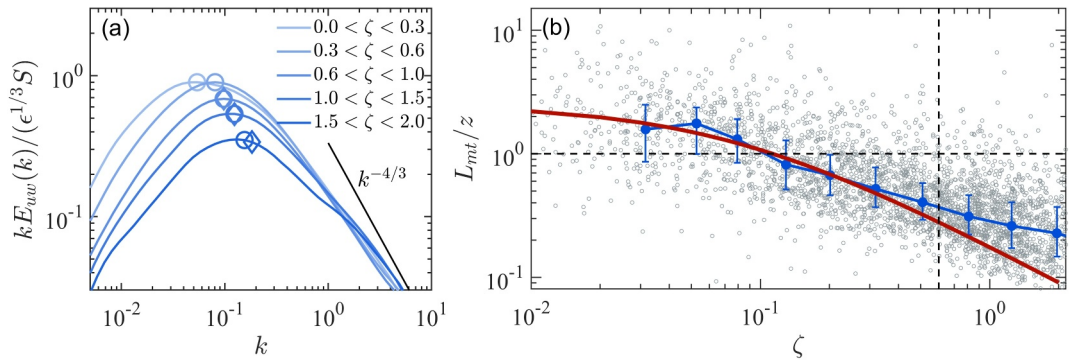

Figure 1. (a) The pre-multiplied co-spectra of momentum flux $E_{uw}(k)$ categorized into five ζ bins. The circles and diamonds on the lines denote the bin-median wavenumbers k_{mt} and k_0, respectively. The black line denotes −7/3 co-spectral scaling (Li & Katul, 2017). (b) The ratio of L_{mt}/z against ζ. The blue dots represent median values in the bins and the vertical bars represent the corresponding upper and lower quartiles. The red solid line denotes the relation $L_{mt}/z = 2.5/(1 + 13.3\zeta)$. The horizontal dashed lines denote unity for reference. The vertical dashed line denotes $\zeta = 0.6$.

pre-multiplied co-spectra of momentum flux averaged over five stability bins, which contain 931, 624, 737, 699, and 424 samples, respectively, are shown in Figure 1a. The corresponding bin-median k_{mt} values are also highlighted in Figure 1a.

2.4. Length Scales

Following previous studies (Caulfield, 2021; Mater et al., 2013; Mater & Venayagamoorthy, 2014a, 2014b), we consider the following parameter space: z; three parameters related to the intrinsic properties of turbulence: ϵ, σ_u, and σ_w, where σ_u indicates the standard deviation of the streamwise velocity; and two parameters related to the mean flow: N and S. The standard deviation of the spanwise velocity σ_v is absent because σ_v is of the same order as σ_w. Based on these parameters, we establish nine fundamental length scales: the measurement height z, the Corrsin length scale $L_c = \left(\epsilon/S^3\right)^{1/2}$ (Corrsin, 1958), the Ozmidov length scale $L_{oz} = \left(\epsilon/N^3\right)^{1/2}$, two shear length scales $L_{uS} = \sigma_u/S$ and $L_{wS} = \sigma_w/S$, two buoyancy length scales $L_{uN} = \sigma_u/N$ and $L_{wN} = \sigma_w/N$, and two turbulent length scales $L_{u\epsilon} = \sigma_u^3/\epsilon$ and $L_{w\epsilon} = \sigma_w^3/\epsilon$. Other length scales can be obtained by combinations of these fundamental scales. The correspondence between L_{mt} and the above mentioned nine length scales is examined using the Wilcoxon rank sum test, which tests the hypothesis that two sets of samples are from continuous distributions with equal medians. The advantage of this test is that it does not rely on specific data distribution assumptions.

3. Results

Moving from neutral conditions, turbulent coherent structures, such as very-large-scale motions (Ghannam et al., 2018; Guala et al., 2011) and attached eddies (Banerjee et al., 2016; Drobinski et al., 2004; Ghannam et al., 2018; Krug et al., 2019), the latter of which scale with z, are gradually deformed due to increasing stability. This causes the deviation of L_{mt} from its scaling at $\zeta = 0$. By averaging data points of L_{mt}/z in the range $-0.01 < \zeta < 0.01$, we find that $L_{mt}/z \approx 1/\kappa = 2.5$ under neutral conditions. For ζ values much smaller than unity, the deviation of L_{mt} from its scaling at $\zeta = 0$ can be approximated using Taylor series as:

$$\frac{L_{mt}}{z} \approx \frac{2.5}{1 + C_1\zeta}, \tag{1}$$

where C_1 is a coefficients that needs to be determined by observational data. Data fitting within the bin $0 < \zeta < 0.3$ yields $C_1 = 13.3$ (this value is insensitive to the selection of the ζ bin). The obtained relation is displayed as the red solid line in Figure 1b. It can be seen that Equation 1 is in good agreement with observational data within the range $0 < \zeta < 0.5 \sim 0.6$. As ζ exceeds $0.5 \sim 0.6$, Equation 1 becomes smaller than observational data, indicating the inapplicability of Equation 1. This result is consistent with Mahrt (2007) and Hong et al. (2010), who documented that wave-like non-turbulent flows distort turbulence statistics when ζ exceeds $0.5 \sim 0.6$.

19448007, 2024, 23, Downloaded from https://agupubs.onlinelibrary.wiley.com/doi/10.1029/2024GL111459, Wiley Online Library on [20/12/2024]. See the Terms and Conditions (https://onlinelibrary.wiley.com/terms-and-conditions) on Wiley Online Library for rules of use; OA articles are governed by the applicable Creative Commons License

19448007, 2024, 23, Downloaded from https://agupubs.onlinelibrary.wiley.com/doi/10.1029/2024GL111459, Wiley Online Library on [20/12/2024]. See the Terms and Conditions (https://onlinelibrary.wiley.com/terms-and-conditions) on Wiley Online Library for rules of use; OA articles are governed by the applicable Creative Commons License

As stability increases, z becomes less relevant and the buoyancy frequency N becomes a more compelling parameter in constraining L_{mt}. Early work (Li et al., 2016) used L_{oz}, which represents the largest eddy unaffected by buoyancy. Implicit in the definition of L_{oz} is the balance between the kinetic energy $k_{oz}E_{tke}(k_{oz}) \sim \epsilon^{2/3}k_{oz}^{-2/3}$ and the potential energy $P(k_{oz}) \sim N^2k_{oz}^{-2}$ (Dougherty, 1961; Ozmidov, 1965; Riley & Lindborg, 2008), where $k_{oz} = 1/L_{oz}$ is the Ozmidov wavenumber. This requires that the spectrum of turbulence kinetic energy (TKE) at k_{oz} still follows the $-5/3$ scaling law (Kolmogorov, 1941). We illustrate the pre-multiplied TKE spectra $E_{tke}(k)$, streamwise velocity spectra $E_u(k)$, spanwise velocity spectra $E_v(k)$, and vertical velocity spectra $E_w(k)$ in Figures 2a–2d to check this requirement. As shown in Figure 2a, the $-5/3$ scaling law region in the TKE spectra does not extend up to k_{oz} (denoted as circles), implying that L_{oz} does not necessarily represent the largest eddy unaffected by buoyancy in stable boundary layers (at least in this data set). This failure of L_{oz} is found to be related to the dissimilarity in the shapes of the streamwise, spanwise, and vertical velocity spectra. One can see that only the streamwise spectra at k_{oz} can be approximately described by the $-5/3$ scaling law (Figure 2b), whereas the spanwise and vertical spectra do not follow this scaling (Figures 2c and 2d). The buoyancy length scale $k_{wN} = 1/L_{wN}$ is similar to k_{oz} in terms of constraining the $-5/3$ scaling law regions (denoted as asterisks in Figures 2a–2d), namely, it works better for the streamwise spectra than the spanwise and vertical spectra. Quantitatively, Figures 2e and 2f present the comparison of L_{oz} and L_{wN} to L_{mt} for individual 15-min segments. Both L_{oz} and L_{wN} appear to be larger than L_{mt}, consistent with the results shown in Figures 2a–2d. Although L_{wN} seems to agree better with L_{mt} than L_{oz}, both the correspondence between L_{mt} and L_{wN} and the correspondence between L_{mt} and L_{oz} are rejected by the Wilcoxon rank sum test at the 5% significance level.

To identify the key parameter controlling this dissimilarity in the shapes of velocity spectra, we derive an equation for $(E_v(k) + E_w(k))/E_u(k)$ based on the Reynolds stress budgets with a focus on the inertial subrange of turbulence (see Text S1), which is expressed as:

$$\frac{E_v(k)+E_w(k)}{E_u(k)} = \frac{8}{3}\frac{1-3/8Ri_gS^2\tau'(k)^2}{1+S^2\tau'(k)^2} \approx \frac{8}{3}\frac{1}{1+S^2\tau'(k)^2}, \tag{2}$$

where $Ri_g = N^2/S^2$ is the gradient Richardson number reflecting the influence of thermal stratification and $\tau'(k)$ is a parameter related to intrinsic properties of turbulence. At high-wavenumber end of the inertial subrange, where the scaling behaviors of $E_u(k)$, $E_v(k)$, and $E_w(k)$ are similar and independent of the background flow, the magnitude of $\tau'(k)$ is negligible to recover a constant $(E_v(k) + E_w(k))/E_u(k) = 8/3$ according to Equation 2. As k decreases, significant deviations of $(E_v(k) + E_w(k))/E_u(k)$ from its constant value at higher wavenumbers (=8/3) occur when $S^2\tau'(k)^2$ becomes on the order of $O(1)$. At this point, $Ri_gS^2\tau'(k)^2 = Ri_gO(1) \ll 1$ given that $Ri_g < 0.2$ when $\zeta < 2$ (Zilitinkevich et al., 2007). Therefore, the dissimilarity in the shapes of the streamwise, spanwise, and vertical velocity spectra is primarily related to S. This is consistent with the fact that the $-5/3$ scaling in the spanwise and vertical spectra seems to end at the shear-related scale $k_{wS} = 1/L_{wS}$ (denoted as triangles in Figures 2c and 2d).

Now we derive an appropriate expression for constraining L_{mt} (denoted as L_0 in this study) by taking into account the dissimilarity in the shapes of the streamwise, spanwise, and vertical velocity spectra. For brevity, two approximations are made: (a) the $-5/3$ scaling in the streamwise spectra extends over $k_0 = 1/L_0$, but the $-5/3$ scaling in the spanwise and vertical spectra ends at k_{wS}; (b) the spanwise and vertical kinetic energy at k_0 are same as those at k_{wS} (see Figure S2 in Supporting Information S1). Then we have the balance between kinetic energy and potential energy at $k_0 = 1/L_0$:

$$\frac{C_u}{2C_{tke}}\epsilon^{2/3}k_0^{-2/3} + 2\frac{C_w}{2C_{tke}}\epsilon^{2/3}k_{wS}^{-2/3} = N^2k_0^{-2}, \tag{3}$$

where $C_u = \frac{18}{55} \times 1.5$, $C_w = \frac{24}{55} \times 1.5$, and $C_{tke} = \frac{33}{55} \times 1.5$ are the coefficients for the one-dimensional horizontal velocity, vertical velocity, and TKE spectra (Pope, 2000), respectively. Note that L_0 recovers L_{oz} by replacing k_{wS} with k_0 in Equation 3. Unfortunately, the solution of Equation 3 is quite complicated. For convenience, we adopt an approximate solution of Equation 3 (see Text S2 in Supporting Information S1), which reads

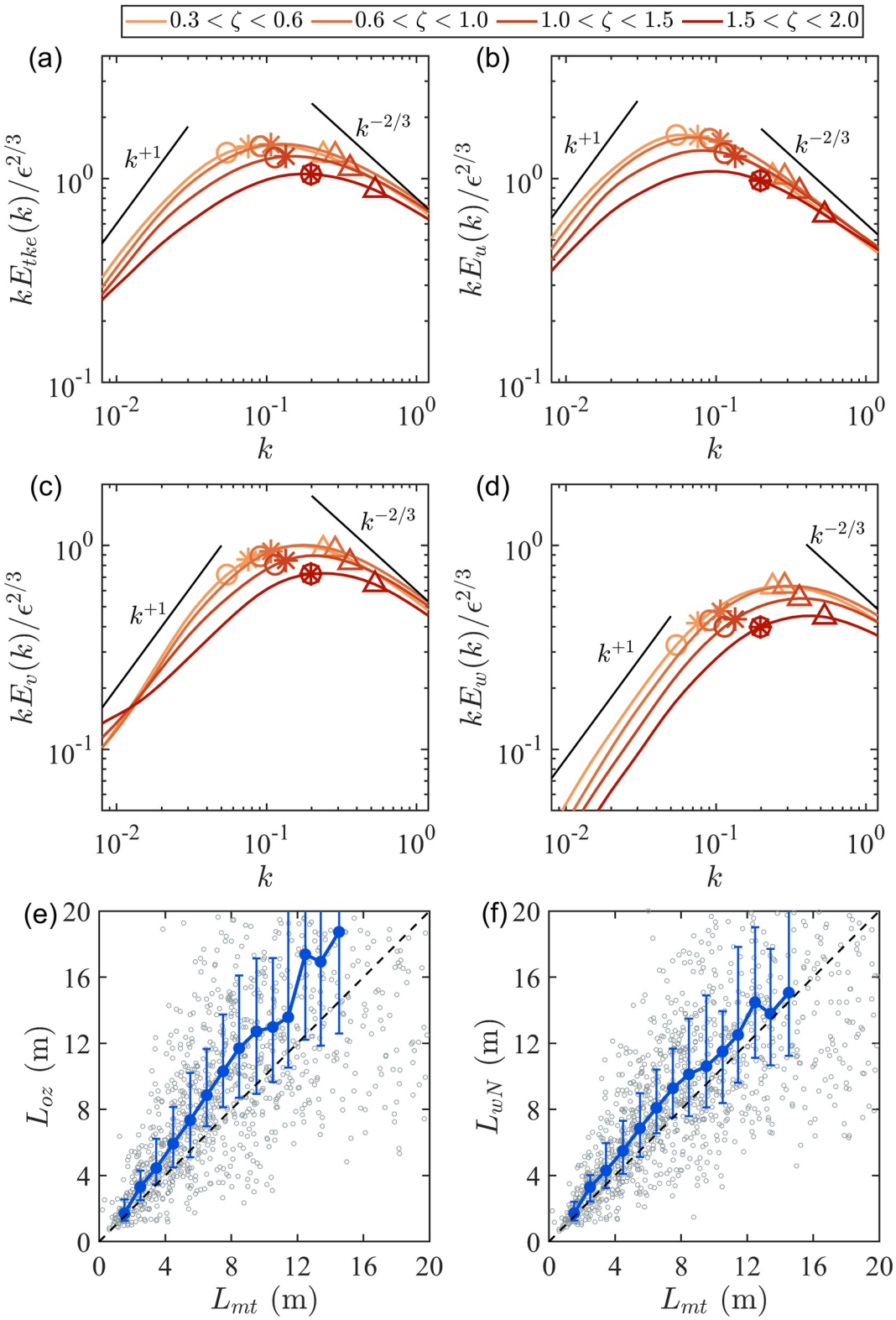

Figure 2.

19448007, 2024, 23, Downloaded from https://agupubs.onlinelibrary.wiley.com/doi/10.1029/2024GL111459, Wiley Online Library on [20/12/2024]. See the Terms and Conditions (https://onlinelibrary.wiley.com/terms-and-conditions) on Wiley Online Library for rules of use; OA articles are governed by the applicable Creative Commons License

19448007, 2024, 23, Downloaded from https://agupubs.onlinelibrary.wiley.com/doi/10.1029/2024GL111459, Wiley Online Library on [20/12/2024]. See the Terms and Conditions (https://onlinelibrary.wiley.com/terms-and-conditions) on Wiley Online Library for rules of use; OA articles are governed by the applicable Creative Commons License

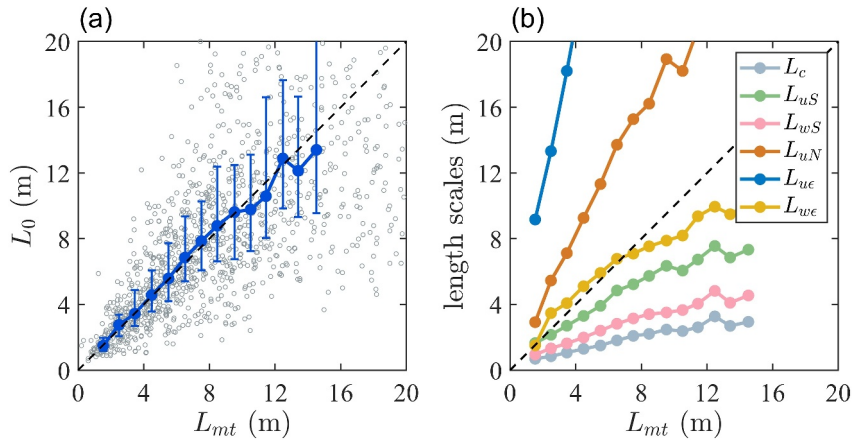

Figure 3. (a) The relationships between L_{mt} and L_0 within the stability range $0.6 < \zeta < 2.0$. The blue dots represent median values in the bins and the vertical bars represent the corresponding upper and lower quartiles. (b) The relationships between L_{mt} and different length scales within the stability range $0.6 < \zeta < 2.0$. The dots represent median values in the bins. The dashed lines indicate 1:1 comparison.

$$L_0 = L_{oz}\left(0.38 + \sqrt{\ln\left(1 + 0.47\frac{L_{wS}}{L_{oz}}\right)}\right). \tag{4}$$

When L_{wS} is equal to L_{oz}, L_0 recovers L_{oz} in Equation 4. Figure S2 in Supporting Information S1 shows the location of L_0 in the TKE, streamwise velocity, spanwise velocity, and vertical velocity spectra. It can be seen that L_0 better demarcates the scale where the $-5/3$ scaling ends than L_{oz}. Figure 1a further shows the location of L_0 on the co-spectra of momentum flux for the stability range $0.6 < \zeta < 2.0$.

One might be attempted to improve L_{wN} by also considering the dissimilarity in the energy spectra. However, this is not possible since L_{wN} arises from the balance between the integrated kinetic energy (instead of scale-wise kinetic energy as in the case of L_{oz}) with potential energy, namely, $\sigma_w^2 \sim N^2 k_{wN}^{-2} = N^2 L_{wN}^2$. Because of this integrated representation of kinetic energy in the formulation of L_{wN}, the dissimilarity in the scale-wise energy distribution cannot be easily incorporated into L_{wN}.

As shown in Figure 3a, one can see that L_{mt} aligns well with L_0, demonstrating a significant improvement over L_{oz} (and L_{wN}) when considering the dissimilarity in the shapes of velocity spectra. The correspondence between L_{mt} and L_0 is accepted by the Wilcoxon rank sum test, suggesting that L_{mt} is better described by L_0 within the stability range $0.6 < \zeta < 2.0$. Other fundamental length scales in Section 2.4 are also compared against L_{mt} in Figure 3b. We find that none of them performs better than L_0, and none passes the Wilcoxon rank sum test.

4. Conclusions and Discussion

Understanding of L_{mt} is important for parametrizing stably stratified turbulence in atmospheric boundary layers. As L_{oz} represents the largest eddy unaffected by buoyancy, previous studies have utilized L_{oz} to parameterize L_{mt} under z-less conditions. This study aims to revisit the applicability and limitations of L_{oz} in characterizing L_{mt}, and provide a comprehensive characterization for L_{mt}. Using the CASES-99 data set, we find that z is relevant in constraining L_{mt} in weakly stable conditions ($0 < \zeta < 0.6$) and less relevant in moderately stable conditions ($0.6 < \zeta < 2.0$). We reveal that L_{oz} does not necessarily represent the largest eddy unaffected by buoyancy under z-less conditions, because it does not constrain the $-5/3$ scaling law regions in the spanwise

Figure 2. (a)–(d) The pre-multiplied spectra of (a) TKE $E_{tke}(k)$, (b) streamwise velocity $E_u(k)$, (c) spanwise velocity $E_v(k)$, and (d) vertical velocity $E_w(k)$ in four ζ bins. The circles, asterisks, and triangles denote the median k_{oz}, k_{wN}, and k_{wS} within the bins, respectively. The black lines indicate the k^{+1} and $k^{-2/3}$ scalings (e)–(f) The relationships between L_{mt} and (e) L_{oz} and (f) L_{wN} within the stability range $0.6 < \zeta < 2.0$. The blue dots represent median values in the bins and the vertical bars represent the corresponding upper and lower quartiles. The dashed lines indicate 1:1 comparison. Only length scales smaller than 20 m are shown as $L_{mt}(\zeta = 0.6) = 15$ m for the highest measurement level ($z = 55$ m) according to Equation 1; moreover, the amount of data for $L_{mt} > 20$ m accounts for only 8% of the total amount of data.

and vertical velocity spectra. Instead, shear-related length scale L_{wS} is more effective in constraining the −5/3 scaling law regions in these velocity spectra. Based on the dissimilarity of velocity spectra and the balance between kinetic energy and potential energy at L_{mt}, we propose that the scale constraining L_{mt} should be expressed as $L_0 = L_{oz}\left(0.38 + \sqrt{\ln(1 + 0.47L_{wS}/L_{oz})}\right)$. We find that L_0 better describes L_{mt} within the stability range $0.6 < \zeta < 2.0$.

Given that current similarity theories are less satisfactory in stable boundary layers (Grachev et al., 2013; Mahrt, 2014), this study has significant implications for boundary layer parameterization schemes. The momentum flux can be obtained by integrating the co-spectrum over the −7/3 scaling region and the production region, which are separated by L_{mt}. Therefore, knowledge of L_{mt} is important for developing parameterizations for momentum transfer. However, it was reported that a sub-region, spanning a wide range of scales from the −7/3 scaling region to the production region, contributes significantly to momentum flux (Li & Katul, 2017). This sub-region needs further investigation. Also, the weak turbulence regime under strongly stable conditions where turbulent mixing is suppressed remains a challenge (Acevedo et al., 2016; Lan et al., 2018; Peltola et al., 2021; Sun et al., 2012, 2016, 2020; Van de Wiel et al., 2012). Shao et al. (2023) found that turbulence in this regime is sliced into thin layers by stratification, resulting in highly anisotropic pancake vortices (Billant & Chomaz, 2000a, 2000b, 2000c). This situation is further complicated by the prevalence of the mesoscale motions (Mahrt et al., 2009; Mahrt & Mills, 2009; Schiavon et al., 2020). Therefore, the applicability of L_0 under very stable conditions is questionable, and the characterization for L_{mt} requires further investigation. Additionally, turbulence under such conditions might be non-stationary with key controlling length scales changing strongly with time. Addressing these knowledge gaps is recommended for future studies.

Data Availability Statement

The CASES-99 data set used in this study for turbulence variable calculation can be downloaded at https://www.eol.ucar.edu/content/integrated-surface-flux-facility-during-cases99.

Acknowledgments
This study is supported by the National Natural Science Foundation of China (Grant 423B2502, U2342221, and 42275065), key innovation team of China Meteorological Administration (CMA2022ZD09), and Science Foundation of Jiangsu Meteorological Bureau (ZD202427). DL acknowledges support from the US-National Science Foundation (NSF) under the Award number AGS-1853354.

References

Acevedo, O. C., Mahrt, L., Puhales, F. S., Costa, F. D., Medeiros, L. E., & Degrazia, G. A. (2016). Contrasting structures between the decoupled and coupled states of the stable boundary layer. *Quarterly Journal of the Royal Meteorological Society*, *142*(695), 693–702. https://doi.org/10.1002/qj.2693

Ayet, A., & Katul, G. G. (2020). Scaling laws for the length scale of energy-containing eddies in a sheared and thermally stratified atmospheric surface layer. *Geophysical Research Letters*, *47*(23). https://doi.org/10.1029/2020gl089997

Banerjee, T., Li, D., Juang, J.-Y., & Katul, G. (2016). A spectral budget model for the longitudinal turbulent velocity in the stable atmospheric surface layer. *Journal of the Atmospheric Sciences*, *73*(1), 145–166. https://doi.org/10.1175/jas-d-15-0066.1

Billant, P., & Chomaz, J.-M. (2000a). Experimental evidence for a new instability of a vertical columnar vortex pair in a strongly stratified fluid. *Journal of Fluid Mechanics*, *418*, 167–188. https://doi.org/10.1017/s0022112000001154

Billant, P., & Chomaz, J.-M. (2000b). Theoretical analysis of the zigzag instability of a vertical columnar vortex pair in a strongly stratified fluid. *Journal of Fluid Mechanics*, *419*, 29–63. https://doi.org/10.1017/s0022112000001166

Billant, P., & Chomaz, J.-M. (2000c). Three-dimensional stability of a vertical columnar vortex pair in a stratified fluid. *Journal of Fluid Mechanics*, *419*, 65–91. https://doi.org/10.1017/s0022112000001178

Businger, J. A., Wyngaard, J. C., Izumi, Y., & Bradley, E. F. (1971). Flux-Profile relationships in the atmospheric surface layer. *Journal of the Atmospheric Sciences*, *28*(2), 181–189. https://doi.org/10.1175/1520-0469(1971)028<0181:Fprita>2.0.Co;2

Caulfield, C. P. (2021). Layering, instabilities, and mixing in turbulent stratified flows. *Annual Review of Fluid Mechanics*, *53*(1), 113–145. https://doi.org/10.1146/annurev-fluid-042320-100458

Corrsin, S. (1958). *Local isotropy in turbulent shear flow* (Vol. 34). National Advisory Committee for Aeronautics.

Dougherty, J. P. (1961). The anisotropy of turbulence at the meteor level. *Journal of Atmospheric and Terrestrial Physics*, *21*(2–3), 210–213. https://doi.org/10.1016/0021-9169(61)90116-7

Drobinski, P., Carlotti, P., Newsom, R. K., Banta, R. M., Foster, R. C., & Redelsperger, J.-L. (2004). The structure of the near-neutral atmospheric surface layer. *Journal of the Atmospheric Sciences*, *61*(6), 699–714. https://doi.org/10.1175/1520-0469(2004)061<0699:Tsotna>2.0.Co;2

Dyer, A. J. (1974). A review of flux-profile relationships. *Boundary-Layer Meteorology*, *7*(3), 363–372. https://doi.org/10.1007/bf00240838

Foken, T. (2006). 50 Years of the Monin–Obukhov similarity theory. *Boundary-Layer Meteorology*, *119*(3), 431–447. https://doi.org/10.1007/s10546-006-9048-6

Ghannam, K., Katul, G. G., Bou-Zeid, E., Gerken, T., & Chamecki, M. (2018). Scaling and similarity of the anisotropic coherent eddies in near-surface atmospheric turbulence. *Journal of the Atmospheric Sciences*, *75*(3), 943–964. https://doi.org/10.1175/jas-d-17-0246.1

Grachev, A. A., Andreas, E. L., Fairall, C. W., Guest, P. S., & Persson, P. O. G. (2013). The critical Richardson number and limits of applicability of local similarity theory in the stable boundary layer. *Boundary-Layer Meteorology*, *147*(1), 51–82. https://doi.org/10.1007/s10546-012-9771-0

Grachev, A. A., Andreas, E. L., Fairall, C. W., Guest, P. S., & Persson, P. O. G. (2015). Similarity theory based on the Dougherty-Ozmidov length scale. *Quarterly Journal of the Royal Meteorological Society*, *141*(690), 1845–1856. https://doi.org/10.1002/qj.2488

Guala, M., Metzger, M., & McKeon, B. J. (2011). Interactions within the turbulent boundary layer at high Reynolds number. *Journal of Fluid Mechanics*, *666*, 573–604. https://doi.org/10.1017/s0022112010004544

19448007, 2024, 23, Downloaded from https://agupubs.onlinelibrary.wiley.com/doi/10.1029/2024GL111459, Wiley Online Library on [20/12/2024]. See the Terms and Conditions (https://onlinelibrary.wiley.com/terms-and-conditions) on Wiley Online Library for rules of use; OA articles are governed by the applicable Creative Commons License

Högström, U. (1988). Non-dimensional wind and temperature profiles in the atmospheric surface layer: A re-evaluation. *Boundary-Layer Meteorology*, *42*(1–2), 55–78. https://doi.org/10.1007/bf00119875
Holtslag, A. A. M., & Nieuwstadt, F. T. M. (1986). Scaling the atmospheric boundary layer. *Boundary-Layer Meteorology*, *36*(1–2), 201–209. https://doi.org/10.1007/bf00117468
Hong, J., Kim, J., Ishikawa, H., & Ma, Y. (2010). Surface layer similarity in the nocturnal boundary layer: The application of Hilbert-Huang transform. *Biogeosciences*, *7*(4), 1271–1278. https://doi.org/10.5194/bg-7-1271-2010
Ji, Y., & Chen, X. (2023). Symmetry analysis of mean velocity distribution in stratified atmospheric surface layers. *Symmetry*, *15*(10), 1951. https://doi.org/10.3390/sym15101951
Katul, G. G., Konings, A. G., & Porporato, A. (2011). Mean velocity profile in a sheared and thermally stratified atmospheric boundary layer. *Physical Review Letters*, *107*(26), 268502. https://doi.org/10.1103/PhysRevLett.107.268502
Katul, G. G., Porporato, A., Manes, C., & Meneveau, C. (2013). Co-spectrum and mean velocity in turbulent boundary layers. *Physics of Fluids*, *25*(9). https://doi.org/10.1063/1.4821997
Katul, G. G., Porporato, A., Shah, S., & Bou-Zeid, E. (2014). Two phenomenological constants explain similarity laws in stably stratified turbulence. *Physical Review E - Statistical, Nonlinear and Soft Matter Physics*, *89*(2), 023007. https://doi.org/10.1103/PhysRevE.89.023007
Klipp, C. (2014). Turbulence anisotropy in the near-surface atmosphere and the evaluation of multiple outer length scales. *Boundary-Layer Meteorology*, *151*(1), 57–77. https://doi.org/10.1007/s10546-013-9884-0
Kolmogorov, A. N. (1941). The local structure of turbulence in incompressible viscous fluid for very large Reynolds numbers. *Doklady Akademii Nauk SSSR*, *30*, 299–303.
Krug, D., Baars, W. J., Hutchins, N., & Marusic, I. (2019). Vertical coherence of turbulence in the atmospheric surface layer: Connecting the hypotheses of Townsend and davenport. *Boundary-Layer Meteorology*, *172*(2), 199–214. https://doi.org/10.1007/s10546-019-00445-4
Lan, C., Liu, H., Li, D., Katul, G. G., & Finn, D. (2018). Distinct turbulence structures in stably stratified boundary layers with weak and strong surface shear. *Journal of Geophysical Research: Atmospheres*, *123*(15), 7839–7854. https://doi.org/10.1029/2018jd028628
Li, D. (2020). The O'KEYPS equation and 60 Years beyond. *Boundary-Layer Meteorology*, *179*(1), 19–42. https://doi.org/10.1007/s10546-020-00585-y
Li, D., & Katul, G. G. (2017). On the linkage between the k−5/3 spectral and k−7/3 cospectral scaling in high-Reynolds number turbulent boundary layers. *Physics of Fluids*, *29*(6). https://doi.org/10.1063/1.4986068
Li, D., Salesky, S. T., & Banerjee, T. (2016). Connections between the Ozmidov scale and mean velocity profile in stably stratified atmospheric surface layers. *Journal of Fluid Mechanics*, *797*, R3. https://doi.org/10.1017/jfm.2016.311
Mahrt, L. (2007). The influence of nonstationarity on the turbulent flux–gradient relationship for stable stratification. *Boundary-Layer Meteorology*, *125*(2), 245–264. https://doi.org/10.1007/s10546-007-9154-0
Mahrt, L. (2014). Stably stratified atmospheric boundary layers. *Annual Review of Fluid Mechanics*, *46*(1), 23–45. https://doi.org/10.1146/annurev-fluid-010313-141354
Mahrt, L., & Mills, R. (2009). Horizontal diffusion by submeso motions in the stable boundary layer. *Environmental Fluid Mechanics*, *9*(4), 443–456. https://doi.org/10.1007/s10652-009-9126-7
Mahrt, L., Thomas, C. K., & Prueger, J. H. (2009). Space-time structure of mesoscale motions in the stable boundary layer. *Quarterly Journal of the Royal Meteorological Society*, *135*(638), 67–75. https://doi.org/10.1002/qj.348
Marusic, I., & Monty, J. P. (2019). Attached eddy model of wall turbulence. *Annual Review of Fluid Mechanics*, *51*(1), 49–74. https://doi.org/10.1146/annurev-fluid-010518-040427
Mater, B. D., Schaad, S. M., & Venayagamoorthy, S. K. (2013). Relevance of the Thorpe length scale in stably stratified turbulence. *Physics of Fluids*, *25*(7). https://doi.org/10.1063/1.4813809
Mater, B. D., & Venayagamoorthy, S. K. (2014a). A unifying framework for parameterizing stably stratified shear-flow turbulence. *Physics of Fluids*, *26*(3). https://doi.org/10.1063/1.4868142
Mater, B. D., & Venayagamoorthy, S. K. (2014b). The quest for an unambiguous parameterization of mixing efficiency in stably stratified geophysical flows. *Geophysical Research Letters*, *41*(13), 4646–4653. https://doi.org/10.1002/2014gl060571
Mellor, G. L., & Yamada, T. (1974). A hierarchy of turbulence closure models for planetary boundary layers. *Journal of the Atmospheric Sciences*, *31*(7), 1791–1806. https://doi.org/10.1175/1520-0469(1974)031<1791:Ahotcm>2.0.Co;2
Monin, A. S., & Obukhov, A. M. (1954). Basic laws of turbulent mixing in the ground layer of the atmosphere. *Akad. Nauk. SSSR Geofiz. Inst. Trudy*, *151*, 163–187.
Ozmidov, R. (1965). On the turbulent exchange in a stably stratified ocean. *Izvestiya Academy of Sciences USSR, Atmospheric and Oceanic Physics*, *1*, 853–860.
Peltola, O., Lapo, K., & Thomas, C. K. (2021). A physics-based universal indicator for vertical decoupling and mixing across canopies architectures and dynamic stabilities. *Geophysical Research Letters*, *48*(5). https://doi.org/10.1029/2020gl091615
Pope, S. (2000). *Turbulent flows*. Cambridge University Press.
Poulos, G. S., Blumen, W., Fritts, D. C., Lundquist, J. K., Sun, J., Burns, S. P., et al. (2002). CASES-99: A comprehensive investigation of the stable nocturnal boundary layer. *Bulletin of the American Meteorological Society*, *83*(4), 555–581. https://doi.org/10.1175/1520-0477(2002)083<0555:Caciot>2.3.Co;2
Riley, J. J., & Lindborg, E. (2008). Stratified turbulence: A possible interpretation of some geophysical turbulence measurements. *Journal of the Atmospheric Sciences*, *65*(7), 2416–2424. https://doi.org/10.1175/2007jas2455.1
Salesky, S. T., Katul, G. G., & Chamecki, M. (2013). Buoyancy effects on the integral lengthscales and mean velocity profile in atmospheric surface layer flows. *Physics of Fluids*, *25*(10). https://doi.org/10.1063/1.4823747
Sandu, I., Beljaars, A., Bechtold, P., Mauritsen, T., & Balsamo, G. (2013). Why is it so difficult to represent stably stratified conditions in numerical weather prediction (NWP) models? *Journal of Advances in Modeling Earth Systems*, *5*(2), 117–133. https://doi.org/10.1002/jame.20013
Schiavon, M., Tampieri, F., Caggio, M., & Bodnár, T. (2020). Motions on second-order moment budgets in the stable atmospheric boundary layer. In *Paper presented at conference on topical problems of fluid mechanics 2020*. Institute of Thermomechanics of the Czech Academy of Sciences. https://doi.org/10.14311/TPFM.2020.025
Shao, X., Zhang, N., Li, D., & Sun, J. (2023). A non-dimensional index for characterizing the transition of turbulence regimes in stable atmospheric boundary layers. *Geophysical Research Letters*, *50*(18), e2023GL105304. https://doi.org/10.1029/2023GL105304
Shi, Y., & Hu, F. (2020). Ramp-like PM accumulation process and Z-less similarity in the stable boundary layer. *Geophysical Research Letters*, *47*(3). https://doi.org/10.1029/2019gl086530
Sorbjan, Z. (2006). Local structure of turbulence in stably stratified boundary layers. *Journal of the Atmospheric Sciences*, *63*(5), 1526–1537. https://doi.org/10.1175/jas3704.1

19448007, 2024, 23, Downloaded from https://agupubs.onlinelibrary.wiley.com/doi/10.1029/2024GL111459, Wiley Online Library on [20/12/2024]. See the Terms and Conditions (https://onlinelibrary.wiley.com/terms-and-conditions) on Wiley Online Library for rules of use; OA articles are governed by the applicable Creative Commons License

Sun, J., Lenschow, D. H., LeMone, M. A., & Mahrt, L. (2016). The role of large-coherent-eddy transport in the atmospheric surface layer based on CASES-99 observations. *Boundary-Layer Meteorology*, *160*(1), 83–111. https://doi.org/10.1007/s10546-016-0134-0

Sun, J., Mahrt, L., Banta, R. M., & Pichugina, Y. L. (2012). Turbulence regimes and turbulence intermittency in the stable boundary layer during CASES-99. *Journal of the Atmospheric Sciences*, *69*(1), 338–351. https://doi.org/10.1175/jas-d-11-082.1

Sun, J., Takle, E. S., & Acevedo, O. C. (2020). Understanding physical processes represented by the Monin–Obukhov bulk formula for momentum transfer. *Boundary-Layer Meteorology*, *177*(1), 69–95. https://doi.org/10.1007/s10546-020-00546-5

Townsend, A. A. (1976). *The structure of turbulent shear flow* (2nd ed.). Cambridge University Press.

Van de Wiel, B. J. H., Moene, A. F., Jonker, H. J. J., Baas, P., Basu, S., Donda, J. M. M., et al. (2012). The minimum wind speed for sustainable turbulence in the nocturnal boundary layer. *Journal of the Atmospheric Sciences*, *69*(11), 3116–3127. https://doi.org/10.1175/jas-d-12-0107.1

Welch, P. (1967). The use of fast fourier transform for the estimation of power spectra: A method based on time averaging over short, modified periodograms. *IEEE Transactions on Audio and Electroacoustics*, *15*(2), 70–73. https://doi.org/10.1109/tau.1967.1161901

Zilitinkevich, S. S., Elperin, T., Kleeorin, N., & Rogachevskii, I. (2007). Energy- and flux-budget (EFB) turbulence closure model for stably stratified flows. Part I: Steady-state, homogeneous regimes. *Boundary-Layer Meteorology*, *125*(2), 167–191. https://doi.org/10.1007/s10546-007-9189-2

Zilitinkevich, S. S., Elperin, T., Kleeorin, N., Rogachevskii, I., & Esau, I. (2013). A hierarchy of energy- and flux-budget (EFB) turbulence closure models for stably-stratified geophysical flows. *Boundary-Layer Meteorology*, *146*(3), 341–373. https://doi.org/10.1007/s10546-012-9768-8

References From the Supporting Information

Rotta, J. (1951). Statistische theorie nichthomogener Turbulenz. *Zeitschrift fr Physik*, *129*(6), 547–572. https://doi.org/10.1007/bf01330059

Stull, R. B. (1988). *An introduction to boundary layer meteorology*. Kluwer Acad. Publ.

19448007, 2024, 23, Downloaded from https://agupubs.onlinelibrary.wiley.com/doi/10.1029/2024GL111459, Wiley Online Library on [20/12/2024]. See the Terms and Conditions (https://onlinelibrary.wiley.com/terms-and-conditions) on Wiley Online Library for rules of use; OA articles are governed by the applicable Creative Commons License